Mathematical Biosciences 373 (2024) 109207

Contents lists available at ScienceDirect

Mathematical Biosciences

journal homepage: www.elsevier.com/locate/mbs

Review

Mathematical modeling of brain metastases growth and response to therapies: A review

Beatriz Ocaña-Tienda *, Víctor M. Pérez-García

Mathematical Oncology Laboratory (MOLAB), University of Castilla-La Mancha, Avda. Camilo José Cela s/n, 13071, Ciudad Real, Spain

ARTICLE INFO

Keywords:
Mathematical oncology
Mathematical models
Brain metastases
Brain tumors
Radiation necrosis

ABSTRACT

Brain metastases (BMs) are the most common intracranial tumor type and a significant health concern, affecting approximately 10% to 30% of all oncological patients. Although significant progress is being made, many aspects of the metastatic process to the brain and the growth of the resulting lesions are still not well understood. There is a need for an improved understanding of the growth dynamics and the response to treatment of these tumors. Mathematical models have been proven valuable for drawing inferences and making predictions in different fields of cancer research, but few mathematical works have considered BMs. This comprehensive review aims to establish a unified platform and contribute to fostering emerging efforts dedicated to enhancing our mathematical understanding of this intricate and challenging disease. We focus on the progress made in the initial stages of mathematical modeling research regarding BMs and the significant insights gained from such studies. We also explore the vital role of mathematical modeling in predicting treatment outcomes and enhancing the quality of clinical decision-making for patients facing BMs.

1. Introduction

Brain metastases (BMs) are the most common intracranial tumors in adults with an incidence of around 10% to 30% of all oncological patients [1,2]. Autopsy studies have revealed that 30%–40% of cancer patients had BMs, suggesting that the true prevalence could be larger [3]. In the United States alone, the number of patients affected by BMs was around 250,000 in 2021 [4]. The figures of BM diagnoses are increasing which could be attributed to two primary factors. Firstly, medical imaging technology has improved, enabling better resolution and detection of even small metastases. Secondly, the increasing number of patients affected by primary cancers and their longer survival could contribute to the overall increase in BM cases [2,5].

These statistics reveal that BMs represent a disease burden comparable to that of the most common cancers, such as prostate, breast, or lung cancer. Despite the significant number of patients affected by BMs, the number of active prospective studies in 2021 was fewer than 200. In contrast, there were over 1000 active prospective studies in prostate cancer and nearly 2000 in lung cancer [4].

The metastatic process in the brain starts with individual tumor cells or cell clusters that move from a primary site to the brain. Typically, these cells invade the surrounding tissue and travel through the bloodstream from the original tumor site. Upon reaching the brain, metastatic cells come to a halt at branch points in microvessels, then move out of vessels, and remain nearby to microvessels, when they expand by vessel cooption [6,7]. Their growth is possible if they can evade the immune system and adapt to their new environment [8]. When cancerous cells line up alongside capillaries, they create elongated clusters of metastatic cells called micrometastases [9]. The colonization of brain cells is a lengthy and highly inefficient process. This is due to the fact that the majority of cells that invade the brain die [10]. While the mechanisms governing the initial phases of tumor cell dispersion [11] and the later stages of macrometastatic development are relatively well understood [12,13], the factors determining the survival and successful adaptation of cancer cells that have spread to the brain remain partially unknown, and a substantial amount of basic biological research is being developed to obtain a deeper understanding of these processes.

The advent of mathematical modeling has presented a promising avenue for unraveling the complex interplay of many biological elements in cancers. Its application in this field has garnered recognition due to its potential to provide deeper insights into the mechanisms governing cancer development, pinpoint potential targets for therapy, and generate novel hypotheses [14]. Beyond that, mathematical models offer the opportunity to fine-tune drug dosing and scheduling, leading to enhanced treatment efficacy and minimized toxicity [15]. Consequently, the integration of mathematical modeling in cancer research holds the power to advance the field, paving the path toward more efficient and personalized treatment approaches.

* Corresponding author.
E-mail addresses: Beatriz.Ocana@uclm.es (B. Ocaña-Tienda), Victor.PerezGarcia@uclm.es (V.M. Pérez-García).

https://doi.org/10.1016/j.mbs.2024.109207
Received 23 September 2023; Received in revised form 4 April 2024; Accepted 10 May 2024
Available online 15 May 2024

Mathematical models have been widely used in the study of primary brain tumors, specifically gliomas such as glioblastoma multiforme (GBM) or low-grade gliomas (LGGs). A wide variety of model types has been utilized to capture the complexities of GBM, ranging from ordinary differential equations (ODEs) [16–18] to partial differential equations (PDEs) [19–21], stochastic differential equations (SDEs) [22], cellular automata (CA) [23–25], and evolutionary game theory models (EGTs) [26]. Through these diverse methods, mathematical models have successfully addressed various aspects of GBM, shedding light on critical points such as the tumor's response to chemo- and radiotherapy [27–38], or other types of treatments [39–43], the development of resistances [44–46], as well as phenotypic changes induced by treatments [47–49]. Moreover, mathematical models have been used to identify biomarkers with prognostic value [50–54]. However, despite the much larger incidence of BMs over primary brain tumors, the number of studies devoted to using mathematical tools to understand BMs has been very limited.

Mathematical models have been previously employed to study the metastatic process, encompassing various aspects such as the growth and dissemination of untreated metastases [55–59], extravasation [58,60–62], interactions between primary and secondary tumors [63–67], and therapeutic strategies [68,69]. Nonetheless, BMs exhibit unique characteristics that distinguish them from other types of metastases, primarily due to the presence of the blood–brain barrier. This barrier acts as a formidable obstacle, preventing the entry of foreign substances and cells into the brain and posing a significant challenge for research in this area. Moreover, BMs differ from GBMs in several key aspects. They demonstrate less infiltrative behavior, tend to be smaller in size on diagnosis, and their molecular origins are substantially different, leading to distinct clinical courses and management approaches. These distinctions make the study of BMs a specialized and important area of focus in oncology research.

A previous review by Peng et al. [70] addressed computational models in conjunction with bioinformatics techniques and statistical models. The aim of the present review is to highlight the applications of mathematical models in the study of BMs since the development of effective preventive or therapeutic strategies for metastatic cancer requires a comprehensive understanding of the underlying mechanisms at each stage of the metastatic cascade.

This paper reviews 16 research studies, outlined in Table 1, that have addressed different aspects of the formation, growth, and response to treatments of BMs using mathematical tools.

2. Models of the initial stages of BM development

2.1. A model for BM development linked to primary tumor growth

Bilous et al. [71] described the development of BMs as a process dependent on the primary tumor growth. The authors studied different types of mathematical models by combining several biological considerations. The different scenarios studied in the model correspond to different biological assumptions and are summarized in Fig. 1: (a) A model where BMs are disseminated just by primary tumors (PT) and using the same parameters for PT and BM growth. (b) A model with different parameters for PT and BMs. (c) A model with secondary dissemination, where BMs are able to disseminate new BMs. (d) A model with delayed dissemination. (e) A model with BM dormancy phases.

Primary tumor description. To describe primary tumor growth the authors assumed that the number of cells in the primary tumor $S_p(t)$ before treatment $t < T_d$ follows the Gompertz growth model, i.e.

$$\frac{\partial S_p}{\partial t} = \alpha_{0,p} S_p - \beta_p \ln(S_p) S_p, \qquad \forall t < T_d, \tag{1a}$$

where time $t = 0$ corresponds to appearance of the first cancer cell $S_p(t = 0) = 1$, $\alpha_{0,p}$ is the specific growth rate ($\frac{1}{S_p}\frac{dS_p}{dt}$) at this time and β_p is the exponential rate of decrease of the specific growth rate.

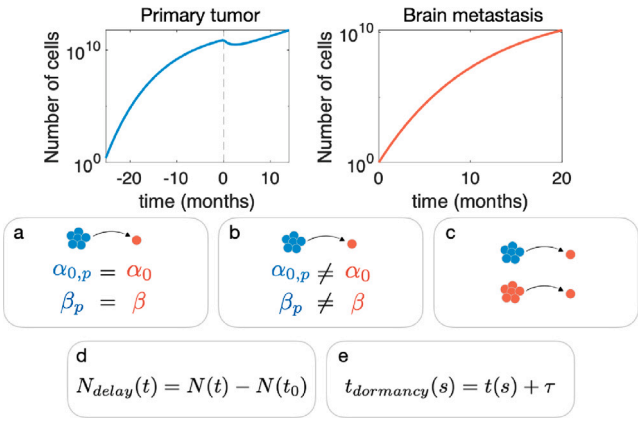

Fig. 1. Scenarios studied by Bilous et al. [71]. Brain metastasis (BM) development was assumed to be dependent on the primary tumor, having both lesions a Gompertzian growth. Five models were defined and studied corresponding to different scenarios: (a) Primary tumors (PTs) are the only source of BMs and the same growth dynamics is assumed for BMs and PTs. (b) The growth of PT and BMs may be different. (c) BMs can give place to new BMs. (d) A delayed dissemination is considered. And (e) a dormancy phase is taken into account.

After treatment starts at $t = T_d$, the number of tumor cells was assumed to follow an exponential growth with growth rate α_1, a log-kill effect of the therapy with parameter of efficacy κ and an exponential decrease of the treatment effect due to resistance, with half-life t_{res} is incorporated in their model, i.e.

$$\frac{\partial S_p}{\partial t} = \alpha_1 S_p - \kappa e^{-\frac{t-T_d}{t_{res}} \ln 2} S_p, \qquad \forall t \geq T_d. \tag{1b}$$

Description of the metastatic process. To incorporate both phases of metastasis development – dissemination and colonization – into their model, the authors based their work on the framework established by Iwata et al. [87]. That led to the formulation of Eq. (2). The dissemination rate d, i.e., the number of successfully born BMs per unit of time, is a function of the number of cells in the primary tumor S_p and is described by

$$d(S_p) = \mu S_p^{\gamma}, \tag{2a}$$

where μ is the probability of cells overcoming the BM formation process and the parameter γ specifies the geometric location of cells that can create a BM across the primary tumor. Assuming the surface cells of the primary tumor as the source, $\gamma = 2/3$. A Gompertzian growth rate $g(s)$ is assumed

$$g(s) = (\alpha_0 - \beta \ln(s))s, \tag{2b}$$

where s is the size of the metastasis and α_0 and β are the growth parameters that depending on the scenario could be equal or different to the ones for the primary tumor $\alpha_{0,p}$ and β_p.

The authors introduced a size-structured density $\rho(t, s)$ to model the population of metastases. The transport partial differential equations describing the density ρ are

$$\partial_t \rho(t, s) + \partial_s(\rho(t, s) g(s)) = 0, \tag{3a}$$

$$g(S_0)\rho(t, S_0) = d(S_p), \tag{3b}$$

where $s \in (S_0, +\infty)$ with S_0 represents the size of a BM at birth (one cell) and $g(t = 0) = 0$. The most significant quantity in the study was the number of visible lesions, i.e. the number $f(t, S_{vis})$ of BMs with sizes larger than 5 mm. The size threshold for BM detection can vary between studies and depending on the resolution of the medical images used. Nonetheless, several studies have supported 5 mm as a common threshold [88,89]. The number of BMs (> 5 mm) $f(t, S_{vis})$ is given by

$$f(t, S_{vis}) = \int_{t(S_{vis})}^{\infty} \rho(t, s')\, ds', \tag{4}$$

Table 1
List of papers reviewed. This summary contains the year of publication, aspects of BMs behavior explored, and type of mathematical model used for the analysis. Abbreviations: BMs — Brain Metastases, ODE — Ordinary Differential Equation, PDE — Partial Differential Equation, RN — Radiation Necrosis.

Reference	Year	Study focus	Type of Mathematical Model
Bilous et al. [71]	2019	Formation of BMs	PDEs
Benzekry et al. [72]	2023	Formation of BMs	PDEs
Smith et al. [73]	2016	Formation of BMs and preventive therapy	ODEs
Yoo et al. [74]	2011	Growth of untreated BMs	Linear equation
Garcia et al. [75]	2018	Growth of untreated BMs	Linear equation
Kobets et al. [76]	2020	Growth of untreated BMs	Linear equation
Shin et al. [77]	2023	Growth of untreated BMs	ODE
Pérez-García et al. [78]	2020	Growth of untreated BMs	ODE
Ocaña-Tienda et al. [79]	2023	Growth of untreated BMs and response to treatment	ODE
Watanabe et al. [80]	2016	Growth of untreated BMs and response to treatment	ODEs
Nawrocki & Zubik-Kowal [81]	2015	Response to treatment	Reaction–diffusion equations
Butner et al. [82]	2021	Response to treatment	ODEs
León-Triana et al. [83]	2021	Response to treatment and radiation necrosis	ODEs
Dohm et al. [84]	2021	Radiation necrosis	Biophysical model
Ocaña-Tienda et al. [85]	2022	Radiation necrosis versus progression	ODEs
Ocaña-Tienda et al. [86]	2023	Radiation necrosis	ODEs and discrete stochastic simulator

with

$$t(S_{vis}) = -\frac{1}{\beta}\ln\left(1 - \frac{\beta}{\alpha_0}\ln(S_{vis})\right), \tag{5}$$

in the case of Gompertz growth.

In addition to the previously mentioned considerations, the authors accounted for another three scenarios. The first one was assuming that BMs can spread themselves. In that scenario the creation of BMs would depend on the primary tumor but also on other BMs, leading to an additional term in Eq. (3b) [87]. The updated equation is now given by

$$g(S_0)\rho(t, S_0) = d(S_p) + \int_{S_0}^{\infty} d(s)\rho(t, s)\, ds. \tag{6}$$

As a second consideration, they introduced a delay t_0 before the onset of metastatic dissemination, with the number of BMs being determined by

$$f_{delay}(t, s) = N_{delay}(t - t(s)) = N(t - t(s)) - N(t_0). \tag{7}$$

Finally, they included a period of dormancy lasting τ, during which newborn BMs remain at size S_0. The time required to reach any given size s is given by $t_{dorm}(s) = t(s) + \tau$.

The dormancy model (e) provided the most accurate fit to the patient data, although it slightly overestimated the number of small visible BMs at 40 months. The remaining models performed worse in fitting the data, suggesting that their assumptions may not contain enough biological richness to provide valid explanations of BM dynamics. The delayed dissemination model (d) had the second best fit although this had an unrealistic t_d of 6 months".

The authors used the dormancy model to make several clinical predictions. These predictions included estimating the time of initial primary tumor appearance, tracking the emergence of new BMs (both measurable and non-measurable, i.e., less than 5 mm in size), and highlighting the potential of this computational approach as a personalized predictive tool for managing BMs. They even suggested considering preventive whole-brain radiotherapy (WBRT) when invisible lesions are predicted. However, it is appropriate to note that for practical clinical use, these models would need from available diagnostic or initial BM occurrence data for validation and model calibration.

In a subsequent study by the same research group [72], the authors used Eqs. (1a) and (2a) to describe the progression, in terms of number and size, of BMs. They also validated the results with a cohort of 20 patients with non-small cell lung cancer (NSCLC). Their results confirmed the predictive potential of the two model parameters, α and β, which were found to correlate with overall survival.

2.2. The impact of prophylactic cranial irradiation on the formation of BMs

Smith et al. [73] developed a computational model to study the effects of prophylactic cranial irradiation on reducing brain metastases risk and burden in breast cancer. The results were validated with experiments in animal models.

The model incorporated several input parameters that were fitted to match the experimental results. These parameters included the number of disseminated tumor cells in the brain shortly after cell injection, the efficiency with which metastases formed, and the interval between cell injection and when metastases began to proliferate. Such optimization was performed using a negative binomial and a Gaussian distribution.

When a cell gives way to a BM, the BM grows according to the Gompertz equation, where the number of cells in the BM is given by the equation

$$N(t) = N(0)e^{k\left[1-e^{-bt}\right]}, \tag{8}$$

where $N(0) = 1$ is the initial number of cells, b is the growth deceleration, and k is the maximum tumor volume. Both parameters were adjusted from the experimental volume data.

To assess the effect of the radiation, the model also included an equation for the surviving fraction of cells $S(d)$ as a function of the radiation dose d,

$$S(d) = e^{-\alpha d-\beta d^2}. \tag{9}$$

where α and β were determined from the clonogenic survival of the cells in monolayer cultures.

The researchers concluded that the timing of radiation treatment is critical for reducing brain metastases in breast cancer. In the model, early irradiation (a few days after cell injection) significantly reduced the incidence of BMs, consistent with what they found in their animal models.

2.3. Summary of BMs development models

Bilous et al. [71] and Smith et al. [73] present distinct computational models addressing BM development. The model of Bilous et al. [71] showed a predictive value for overall survival associated with the proliferation rate of tumor cells and the probability of metastasis per day per cell. The calculation of such parameters requires molecular gene expression signatures and radiomic features. Smith et al. [73] reproduced the incidence of BMs over time and emphasized the importance of early irradiation for effective prevention.

3. Growth of untreated brain metastases

Understanding the natural growth dynamics of BMs before receiving any treatment is key for developing accurate models of response to treatments. However, it is difficult to obtain quantitative data to develop and validate mathematical models since acquiring longitudinal data for untreated malignant tumors presents significant challenges. Treatment decisions are often made quickly to address the urgency of the situation and that limits substantially the availability of untreated BM growth data in humans. In spite of those limitations, several studies have collected pretreatment imaging data to understand better the growth dynamics of untreated BMs.

3.1. Quantifying growth rates in untreated BMs

Several studies have based their analyses on volumetric BM data collected at two pre-treatment time points. This is the most straightforward type of longitudinal information that can be used to determine pre-treatment tumor growth rates. The four studies reviewed in this subsection collectively address the growth rates of BMs in different primary cancer types. These studies highlight the importance of growth rates in prognosis and also underscore their potential impact on treatment planning and long-term patient outcomes.

Yoo et al. [74] investigated the natural growth rate of BMs by analyzing data from 49 lung cancer patients who developed brain metastases (3.6% of 1372 patients) after undergoing NSCLC (non-small cell lung cancer) resections and during their hospital course. Among the patients studied, 28.6% (14) were at stage I of lung cancer, 20.4% (10) at stage II, and the remaining 51.0% (25) at stage III. Within this group, 27 patients exhibited a single BM, while 22 had multiple BMs. Notably, 34 patients exclusively developed metastases in the brain, whereas 15 had metastases in other organs as well. The authors assumed the initial volume to be zero for all cases due to the absence of visible BMs in the pre-diagnosis MRI scans and used the only time point available — the MRI studies on BM diagnosis-. There were no statistically significant differences in tumor growth rates based on lung cancer stages or the use of chemotherapy. However, the rapid development of BMs within a short period of time suggests that micrometastases may be present in the brain even if they are not detectable on MRI. A serious limitation of this study is that the computation of the growth rates requires two time points and thus the results could be substantially influenced by the author's choice of the first time point/volume.

The study conducted by Garcia et al. [75], aimed to investigate factors influencing the growth of BMs and their potential impact on local control. They analyzed data from 411 BMs in 165 patients who underwent fixed-frame SRS for BMs and had both pretreatment diagnostic brain MRI and SRS-planning MRI scans available. Their results showed that melanoma histology had a higher growth rate ($p = 0.02$), as did larger lesions ($p < 0.001$). Factors such as local control, systemic disease status, primary tumor control, and neurological symptoms were not associated with growth rate. The study also highlighted the importance of considering margin expansions to account for growth between planning MRI and SRS delivery. The fact that larger sizes were associated with faster growth rates was not discussed in detail in the paper but is a very interesting fact and in line with results found in other studies to be discussed in detail later [79].

Kobets et al. [76] conducted a study to explore the natural growth rates of BMs in cancer patients before the initiation of any central nervous system-directed therapy. A total of 18 cancer patients (13 with breast cancer and 5 with lung cancer) were included in the study, involving 29 BMs. The authors observed that breast cancer BMs had faster growth rates than lung cancer metastases. They also performed a comparative analysis of the natural growth rate between patients who had died by the end of the study and those who were still alive. The results showed a significantly faster growth rate of lesions in the deceased group, especially those with larger initial volumes, compared to the cohort of patients who remained alive. However, although the trend was clear, none of the results in this study reached statistical significance ($p = 0.38$, $p = 0.19$, and $p = 0.43$, respectively). While the current findings are promising, additional studies with a larger sample size of lesions would be essential to definitively confirm these results.

The study conducted by Shin et al. [77] aimed to investigate the value of pretreatment tumor growth rate in characterizing metastatic disease. Out of the 1049 metastases examined at baseline, only 372 had pre-baseline measurements available. Since the authors intended to calculate the growth rates for all patients in their database, for the remaining cases (677 lesions), the researchers assumed a volume of 0.1 cm^3 90 days prior to the baseline. Besides, only 11 of 86 patients developed metastases in the brain. The tumor growth rate was calculated using an exponential ordinary differential equation

$$\frac{dV}{dt} = \alpha V. \tag{10}$$

They found that the growth parameter α held significant prognostic value not only for progression-free survival but also for overall survival and observed that higher growth rates were associated with shorter survival times, with a Spearman rank correlation coefficient of $S_P = 0.78$ and a p-value of $p = 0.03$. However, the use of overall survival as an endpoint when studying metastatic patients may not be very appropriate, as patients can pass away due to both the metastasis and the primary tumor. Furthermore, more than half of the patients (64.5%) had only one measurement available, so the authors evaluated the initial volume but not the growth rate.

3.2. Using longitudinal data to evaluate the growth dynamics of untreated BMs

The study by Pérez-García et al. [78] and its subsequent extension by Ocaña-Tienda et al. [79] focused on patients for which imaging data for three time-points before treatment were available. That information allowed them to go beyond growth rates and characterize in more

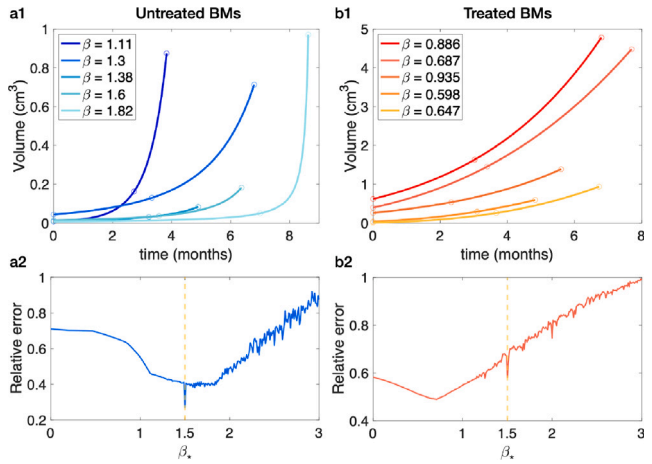

Fig. 2. Growth exponent for brain metastases (BMs): a. before treatment and **b.** recurring after treatment. **1.** Fitting of some patients data according to Eq. (11). **2.** Relative errors obtained when the growth exponent β is fixed for the whole subgroup of untreated ($n = 10$) and recurrent BMs ($n = 72$).
Source: Adapted from [79], Figure 3.

detail the growth law of brain metastasis beyond purely exponential dynamics. In their study, they used the Von-Bertalanffy model [90],

$$\frac{dV}{dt} = \alpha V^{\beta} - bV, \tag{11}$$

to describe the growth of untreated human BMs. Their goal was to find which model in this family (depending on the parameter β) was best fitting the longitudinal growth in their dataset. First, the authors assumed $b \simeq 0$. In the metabolic interpretation of the Von-Bertalanffy model [78] this implies assuming that during tumor growth, energy used in biosynthesis is substantially larger than the one used for basal metabolic maintenance. In this context, a β value of 0 represents linear growth, and a value of 1 represents exponential growth. Thus, any β value greater than 1 represents "accelerating growth". When fitting individual exponents for untreated BMs (Fig. 2.a1), the median value obtained was $\beta = 1.59$ ($n = 10$) suggesting substantial growth acceleration with $\beta \approx 3/2$. When looking for the best growth exponent fitting the subset of untreated patients, $\beta_* = 3/2$ was found to give the best fitting (Fig. 2.a2).

These high values for the growth exponents are likely attributed to the complex evolutionary dynamics within the tumor and the interplay among various cell types, reflecting the tumor's heterogeneity. The authors further validated these findings through in silico simulations employing a stochastic discrete mesoscopic model and analyzing data from experiments in animal models.

3.3. Summary of the growth of untreated BMs

This section outlines studies that focus on understanding the growth dynamics of untreated brain metastases (BMs). The studies were based on either two [74–77] or three time points [78,79]. Although these studies may not have immediate clinical applications, it is crucial to define the natural course of these lesions to guide treatment strategies. Additionally, these studies suggested that melanoma histology and larger lesion size correlate with increased growth rates, and there is evidence of faster growth in breast cancer BMs compared to lung cancer BMs.

4. Mathematical models of brain metastases response to treatments

Because of the poor penetration of most systemic treatments into the brain, the management of BMs has mainly consisted of local therapies such as stereotactic radiotherapy or large-field radiation therapy, along with resection when necessary [91,92]. This is why radiation therapy was the foundation for most reviewed mathematical models that describe the response to treatment.

4.1. Von Bertalaffny-type models to describe the regrowth of treated BMs

After studying untreated BMs (Section 3.2), Ocaña-Tienda et al. [79] also studied data from patients treated with either radiotherapy (RT), chemotherapy (CT), or both and used again the Von-Bertalanffy model given by Eq. (11). The median growth exponent for BMs growing under CT, after completing RT, and for those having received RT and under CT were $\beta = 0.64$ ($n = 16$), 0.72 ($n = 23$) and 0.68 ($n = 33$), respectively. In that study RT includes either whole brain radiation therapy (WBRT), SRT, or a combination of both. Some fittings of the longitudinal growth data of BMs growing after treatment are depicted in Fig. 2.b1.

When looking for the best growth exponent fitting the whole set of treated patients ($n = 72$), $\beta_* = 0.71$ led to the smaller error (Fig. 2.b2). In their conceptual framework, the growth exponent is a measure of the BM evolutionary capabilities, thus the drop in the growth exponent after treatment was interpreted as a treatment-associated reduction in the tumor heterogeneity. Such decrease in heterogeneity after treatment is expected, as the more aggressive (i.e. faster proliferating) subpopulations that drive faster than exponential growth would be more impacted by radiotherapy. This is a very interesting fact since it means that a macroscopic variable (the growth exponent β), that can be obtained from the longitudinal macroscopic dynamics of the BM as observed in MRI images, could provide information on a microscopic variable, the tumor phenotypic/genetic heterogeneity.

4.2. Three models to describe the course of irradiated BMs

Watanabe et al. [80] developed a mathematical model of response to radiation using data from five patients with BMs who had undergone Gamma Knife stereotactic radiosurgery (SRS). They split the longitudinal follow-up of the lesions into three distinct stages. The first phase captured the growth occurring prior to treatment. The second stage represented the period during which the effects of irradiation were actively influencing the system and the last stage represented the period after the effects of the treatment.

To characterize the pre-treatment growth dynamics, the authors considered the total tumor volume V_T to be given by the equations

$$\frac{dV_T}{dt} = \lambda(t)V_T, \tag{12a}$$

$$\frac{d\lambda}{dt} = -\theta\lambda(0)\lambda, \tag{12b}$$

where $\lambda(t)$ is the tumor growth rate, $\lambda(0)$ is the initial tumor growth rate, and θ is the vascular growth retardation factor. While the retardation factor θ was considered to be constant with values between 0.53 and 0.99, the tumor growth rate slows down as the tumor size increases with values between 0.02 days^{-1} and 0.12 days^{-1}. Thus, the current hypotheses lead to the well-known Gompertzian growth for the tumor volume.

After studying the growth of untreated BMs, Watanabe et al. simulated the growth of BMs after irradiation. To define the total tumor volume, the authors included two cell types in the model: the proliferating tumor cells $V_T(t)$ and the non-dividing cells $V_{ND}(t)$.

A single irradiation of dose D applied to the tumor at t_R was assumed. The influence of the radiation was considered to be active for a duration τ_{rad}, which covered the time interval from t_R to $t_R + \tau_{rad}$. After this period, the radiation was assumed to have no further effects on the system.

As illustrated in Fig. 3a, after irradiation and during the period when the radiation effect is active, cells can either transition from proliferating to a non-dividing state at a rate $g(D)$ or remain in a proliferative state at a rate determined by the product of the tumor growth

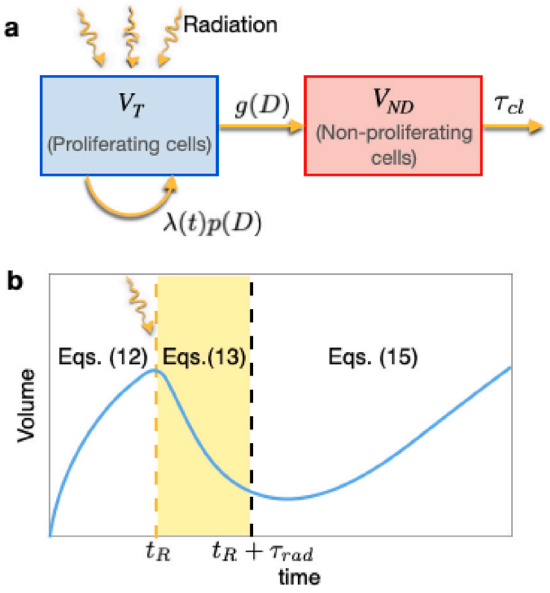

Fig. 3. a. Diagram of the Watanabe et al. model for the period of time when radiation-effect is active, Eq. (13) adapted from [80]. **b.** Schematic representation of the equations used to describe growth and response to treatment over time.

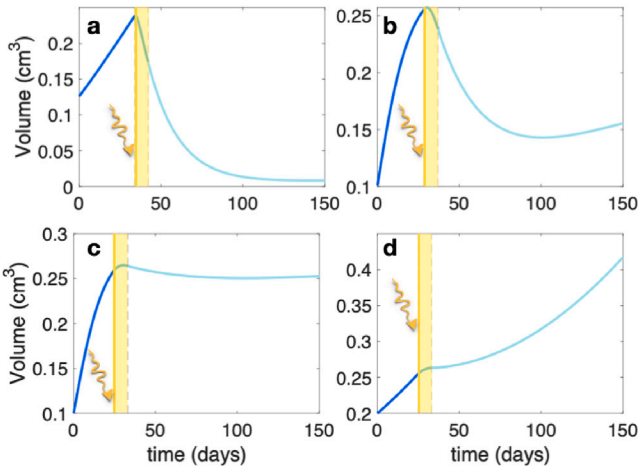

Fig. 4. Examples of simulations for the growth of brain metastases during their follow-up according to Watanabe et al. models: before treatment Eq. (12), when the radiation-effect is active Eq. (13) and after the radiation effect Eq. (15). **a.** Complete response. **b.** Partial response. **c.** Local control. **d.** Treatment failure.

rate $\lambda(t)$ and the cell proliferation probability $p(D)$. Non-dividing cells are removed at a rate τ_{cl}.

The equations describing the tumor volumetric dynamics within the time interval $[t_R, t_R + \tau_{rad}]$ are

$$\frac{dV_T}{dt} = \lambda(t)p(D)V_T - g(D)V_T, \tag{13a}$$

$$\frac{dV_{ND}}{dt} = g(D)V_T - \eta_{cl}V_{ND}, \tag{13b}$$

$$\frac{d\lambda}{dt} = -\theta\lambda(0)\lambda, \tag{13c}$$

where η_{cl} is related to the cell clearance time T_{cl} by $\eta_{cl} = 0.693/T_{cl}$. The probability $p(D)$ and the transition rate of tumor cells from proliferative to non-dividing $g(D)$ are given as functions of the characteristic time T^*, the observation time T_m, and a dose-dependent constant $\chi(D)$, which at the same time is a function of the radiobiological parameters α and α/β and the dose D,

$$p(D) = 1 - \frac{T^*}{3T_m}\chi(D), \tag{14a}$$

$$g(D) = \frac{\chi(D)}{3T_m}, \tag{14b}$$

$$\chi(D) = \alpha D\left(1 + \frac{D}{\alpha/\beta}\right), \tag{14c}$$

with $T^* = 1$ day, $T_m = 10$ days, the radiological parameter $\alpha/\beta = 10$ days and the dose used for the simulation was the prescribed mean dose. The active radiation-effect time τ_{rad} was fixed to 8 days and the authors assumed that λ was constant during that time, then, Eq. (13c) equals to zero.

When the radiation has ceased to affect the system, starting from $t_R + \tau_{rad}$, the tumor growth is defined by

$$\frac{dV_T}{dt} = \lambda(t)V_T, \tag{15a}$$

$$\frac{dV_{ND}}{dt} = -\eta_{cl}V_{ND}, \tag{15b}$$

$$\frac{d\lambda}{dt} = -\theta\lambda(0)\lambda. \tag{15c}$$

During this period, non-proliferative cells are not produced since the radiation is no longer having an effect. The growth is now governed by the same growth that we had before treatment plus the removal of non-proliferative cells.

Some simulations of the model, that cover four typical scenarios after treatment, are illustrated in Fig. 4.

Watanabe's study employed three distinct models, each corresponding to different stages of tumor development: one before treatment (Eq. (12)), another during the radiation-effect phase (Eq. (13)), and a third after the radiation effect (Eq. (15)). These models successfully simulated tumor volume changes observed in BM patients undergoing SRS, effectively replicating clinical data. The study suggested the potential of the model to identify biological parameters that may have predictive value for treatment outcomes.

4.3. A nonlinear reaction–diffusion model to investigate the influence of RT

Nawrocki and Zubik-Kowal [81] developed a nonlinear reaction–diffusion model to describe the spatial and temporal dynamics of a genetically and phenotypically homogeneous BM cell population. Before treatment, the tumor cell density n was assumed to obey a FKPP equation of the form

$$\frac{\partial n}{\partial t} = \nabla\cdot(D\nabla n) + \mu n(1 - n/n_0), \tag{16}$$

where D is the diffusivity of tumor cells in the brain (generally spatially dependent), μ is the cell proliferation rate and n_0 is a reference tumor cell density. The initial condition was assumed to be of the form

$$n(\mathbf{x}, 0) = n_0 e^{-\|\mathbf{x}-\mathbf{x}_0\|^2/\varepsilon}, \tag{17}$$

describing a symmetric cell density distribution with a Gaussian profile. The problem was posed in a spatial domain Ω corresponding to the bounded region in which the BM grows, with no-flux boundary conditions,

$$\mathbf{n}\cdot\mathbf{J} = 0, \tag{18}$$

on the boundary $\partial\Omega$. In Eq. (18) $\mathbf{n}$, is the unit outward normal the boundary $\partial\Omega$ of the domain and $\mathbf{J} = -D\nabla n$ is the diffusive flux of tumor cells.

To account for the radiation effect, the fraction of surviving cells S after each radiation dose d was assumed to depend on the biologically equivalent dose (BED) as

$$S = \exp(-\text{BED}) = \exp\left(-\alpha d - \beta G d^2\right), \tag{19}$$

where the biological parameter α refers to the yield rate for lethal lesions, and β corresponds to the yield rate for sublethal lesions that become lethal as usual in the linear-quadratic response model [93]. The dose protraction factor G, given by

$$G = \frac{2}{d^2}\int_0^t d\tau' I/\tau' \int_0^{\tau'} d\tau I(\tau) e^{-\lambda(\tau'-\tau)}, \tag{20}$$

where $\lambda = \ln(2)/T_{1/2}$ is the repair rate, where $T_{1/2}$ is the half-time for repair and $I(t)$ is the dose rate, related to the cumulated dose delivered by time t. G equals 1 in the linear quadratic model. However, in the case of high radiation doses, which is the case with SRT, this approximation is not accurate. Therefore, G should be reformulated for high dose rates as discussed in [93].

Once the fraction of surviving cells was defined, the model accounted for cell death induced after irradiation, by adding an extra term to Eq. (16) of the form

$$\frac{\partial n}{\partial t} = \nabla \cdot (D\nabla n) + \mu n(1 - n/n_0) - \chi(n, t - t_0), \tag{21}$$

Since radiotherapy was assumed to be applied at $t = t_0$ (and to have no effect for $t < t_0$), the last term in Eq. (21) accounts for those effects. As treatment is expected to reduce cell proliferation, the proliferation rate was allowed to vary after radiation.

Using the model, numerical simulations were conducted to investigate the influence of radiotherapy on the growth dynamics of brain cancer tumors. The simulations accurately reproduced the clinical data across a broad range of values, affirming the mathematical model's potential to accurately depict brain tumor growth dynamics when radiation therapy effects are taken into account.

4.4. A model of immunotherapy response

Butner et al. [82] developed a mathematical model to describe BM response to immune checkpoint inhibitors. In this model, tumor volume changes are characterized by the intrinsic growth of the tumor and the reduction caused by the rate at which cancer cells are eliminated by the treatment, mathematically,

$$\frac{d\rho}{dt} = \rho(\alpha_{\text{baseline}} - \mu + \Lambda\mu) + \rho^2(-\Lambda\mu), \tag{22}$$

where ρ is the normalized tumor volume (with $\rho(0) = 1$), α_{baseline} is the natural tumor growth rate, μ is the kill rate of cancer cells by immune cells, and Λ is the ratio of tumor to immune cells within the tumor, which represents the immune system health state. The long-term solution,

$$\rho^{\infty} = \frac{\alpha_{\text{baseline}} - \mu + \Lambda\mu}{\Lambda\mu} = \frac{\Lambda}{\Lambda\mu}, \tag{23}$$

correlates with the final volume. Finally, the time-dependent solution has the form

$$\rho(t) = \frac{\rho^{\infty}}{1 - (1 - \rho^{\infty})e^{-At}}. \tag{24}$$

The accuracy of the model was demonstrated by its ability to represent the immune response and the final size of 21 BMs together with a patient response classification by ROC curve with an AUC = 0.76. Of particular note, the study conclusions emphasized the importance of the term $\Lambda\mu$, which is directly related to the ratio of tumor volume to immunotherapy efficacy. This relationship depends on variables that can be modified in a clinical setting such as dosing or immune cell fitness, and these modifications can be adjusted to meet the individual needs of each patient. Consequently, the model has the potential to make a significant contribution to the development of personalized treatment plans, which can enhance the overall effectiveness of the immunotherapy treatment.

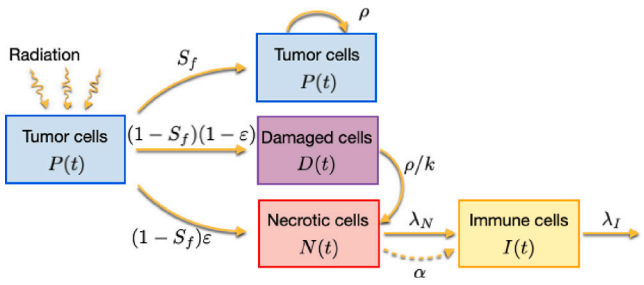

Fig. 5. Schematic representation of the mathematical model constructed by León-Triana et al. ruled by Eqs. (25) and (26).
Source: Figure adapted from [83].

4.5. A compartmental model to capture the response of BMs to radiosurgery

Another model to describe the response of BMs to radiosurgery was developed by León-Triana et al. [83]. Their approach was compartmental but unlike Watanabe et al. model [80], the whole process was described by the same model for all times. The researchers described the dynamics after irradiation with four ordinary differential equations accounting for the dynamics of the different populations. The first one is proliferating tumor cells $P(t)$, assumed to grow exponentially at a rate ρ. The second one is lethally damaged cells $D(t)$, which eventually become necrotic $N(t)$ (third compartment). Finally, necrotic cells activate immune cells $I(t)$ at a rate of α. The immune cells are responsible for clearing out necrotic cells and die at a rate of λ_I, as summarized in Fig. 5.

The equations that govern the response are

$$\frac{dP}{dt} = \rho P, \tag{25a}$$
$$\frac{dD}{dt} = -\frac{\rho}{k} D, \tag{25b}$$
$$\frac{dN}{dt} = \frac{\rho}{k} D - \lambda_N N I, \tag{25c}$$
$$\frac{dI}{dt} = \alpha N - \lambda_I I, \tag{25d}$$

where k represents the average number of mitosis cycles completed before cell death, which is a commonly used hypothesis in mathematical models for various tumor types [94,95], k/ρ gives a time for the death of the population of damaged cells, generally long and λ_N is the constant that modulates the elimination of necrotic cells by the action of immune cells. The initial conditions are

$$P(t_0) = S_f T(t_0), \tag{26a}$$
$$D(t_0) = (1 - S_f)(1 - \varepsilon)T(t_0), \tag{26b}$$
$$N(t_0) = (1 - S_f)\varepsilon T(t_0), \tag{26c}$$
$$I(t_0) = 0, \tag{26d}$$

where S_f is the survival fraction and ε accounts for the fraction of damaged cells that become necrotic directly by the action of the treatment. Simulating the system described in Eq. (25) with the initial conditions given by Eq. (26), leads to a variety of dynamics in agreement with those observed in real patients as exemplified in Fig. 6.a-c.

Thus, this study presented a set of ODEs that effectively captured the longitudinal dynamics of brain metastases after SRS with remarkable accuracy.

4.6. Summary of models for the response to treatment

The examined mathematical models for BMs treatment response offer distinct insights into various therapeutic modalities. The model of Watanabe et al. [80] showed a promising predictive ability regarding volume changes after treatment, based on two key model

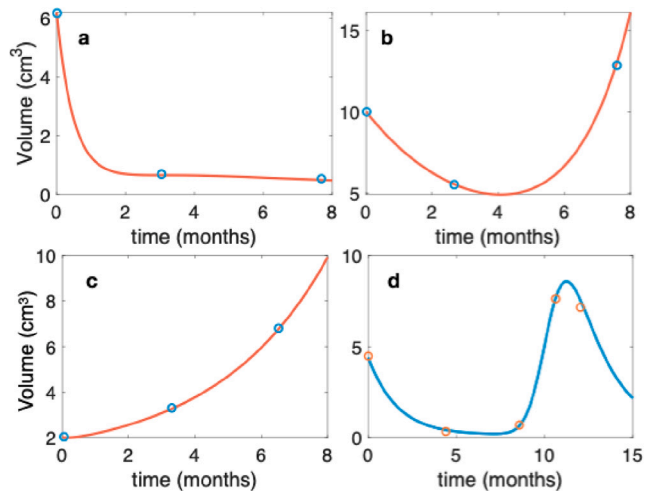

Fig. 6. Fittings of brain metastasis patient response data to stereotactic radiosurgery according to León-Triana et al. [83]. **a-c.** Solutions to Eq. (25) for **a.** a complete response, **b.** a partial response and **c.** a treatment failure. **d.** Solutions to Eqs. (25a)–(25d), (27) in a case in which radiation necrosis was diagnosed. Dots represent volumetric measurements and the continuous lines are the best fits obtained by the model.

parameters: α and θ. α represents a radiological parameter, while θ denotes the vascular growth retardation factor, which represents the deceleration of growth as the tumor expands. Determination of the vascular growth retardation factor requires data from multiple pretreatment time points to provide a comprehensive understanding of each tumor's natural growth trajectory. Butner et al.'s immunotherapy response model demonstrated predictive accuracy of response to therapy based on tumor growth rate and strength of immune response parameters, which are related to clinically modifiable variables such as dosage or immune cell fitness [82]. The remaining models described in this section are devoted to the better understanding on the growth dynamics of BMs after treatment. Ocaña-Tienda et al. [79] showed a decrease in the growth exponent β after treatment, indicating reduced tumor heterogeneity. Nawrocki and Zubik-Kowal's nonlinear reaction–diffusion model provided a broad understanding of BM growth dynamics under irradiation [81]. And León-Triana et al. [83] unified pretreatment, radiation-induced effects, and post-radiation dynamics in the same model, contributing to a comprehensive understanding of BM response to radiosurgery.

5. Mathematical models of radiation necrosis

Radiation necrosis (RN) is the most relevant adverse radiation effect after SRS treatment [96]. It is an inflammatory reaction resulting from vascular damage together with immune activation [97] and it appears between 6 and 24 months following SRS [98,99]. The incidence of RN ranges from 5 to 30% across studies [98,99].

Although RN itself can be managed easily and often resolves spontaneously, it mimics true progression in terms of both appearance and clinical symptoms [100]. Both entities appear as growing contrast-enhanced masses in MR images. However, despite their similarities, treatment options are very different. While RN can often be managed with conservative treatment, avoiding further radiation, progressive tumors may be treated with either repeated SRS or surgical resection [101]. Also, the coexistence of tumor and RN further complicates diagnosis. Biopsy sampling is the gold-standard diagnostic technique for distinguishing tumor progression from RN, however, it is an invasive procedure that has some limitations [102].

5.1. A compartmental model to capture the response of BMs to SRS: RN

To describe radiation necrosis events that occur after radiosurgery, León-Triana et al. [83] adjusted their model's equation that govern the dynamics of necrotic cells Eq. (25c). Necrotic cells resulted from the death of damaged cells and were cleared by immune cells. To incorporate radiation necrosis, they introduced a third term representing healthy cells surrounding the BMs, which are killed by radiation, triggering an inflammatory reaction. The modified equation now reads

$$\frac{dN}{dt} = \frac{\rho}{k} D - \lambda_N N I + h(t), \tag{27}$$

with $h(t) = a \cdot \text{Normal}(\mu, \sigma)$, a Gaussian function. A solution from Eqs. (25a)–(25d), (27) is shown in Fig. 6.d fitting a case of radiation necrosis.

This study presented a mathematical model that effectively describes the response to treatment but also radiation necrosis instances. The model was discussed to hold promise as a potential foundation for biomarkers aimed at distinguishing between radiation necrosis and true progression, but did not address the problem in detail using patient's data.

5.2. A biophysical model for RN

A biophysical model of tumor growth was developed by Dohm et al. to distinguish RN events from tumor progressions [84,103]. The same model had been previously used to describe the response of breast tumors to neoadjuvant chemotherapy [104–106]. The tumor is assumed to have a logistic growth, which is parametrized from postcontrast T1-weighted MR images, while the surrounding tissue, edema visualized on Fluid-Attenuated Inversion Recovery (FLAIR) images, is compared with mechanical stress fields, Fig. 7.

The equations modeling the system are

$$\frac{\partial N(x,t)}{\partial t} = \nabla \cdot (D \nabla N(x,t)) + k N(x,t) \left(1 - \frac{N(x,t)}{\theta}\right), \tag{28a}$$

$$D = D_0 e^{-\gamma \sigma_{VM}(x,t)}, \tag{28b}$$

$$\nabla \cdot \sigma - \lambda \nabla N(x,t) = 0, \tag{28c}$$

with

$$\nabla \cdot \sigma = \nabla \cdot G \nabla \vec{u} + \nabla \frac{G}{1-2\nu} (\nabla \cdot \vec{u}). \tag{29}$$

Eq. (28a) models how the number of tumor cells $N(x,t)$ changes at each location and time as a combination of tumor cell diffusion and logistic growth, where k is the growth rate (dependent of space) and θ is the tumor cell carrying capacity.

Eq. (28b) represents the apparent cell diffusion $D(\sigma_{VM}, x, t)$ linked to the surrounding tissue stiffness/ mechanics, where σ_{VM} is the von Mises stress, γ is an empirically derived coupling constant, and D_0 is the diffusion of tumor cells in the absence of external stress. The von Mises stress describes the loading circumstances brought on by tumor growth. It represents local distortional strain energy. This behavior mimics the mechano-inhibitory effects seen from in vitro and in vivo investigations, which show that cancer cells reduce their diffusivity when in contact with regions of high-stress intensity.

Eq. (28c) describes mechanical equilibrium subject to an external expansive force determined by changes in tumor cell number and a coupling constant λ. This equation governs the response of the displacement vector $\vec{u}$ to tumor cell growth. G represents shear modulus, an intrinsic mechanical property of tumor tissue $G = E/2(1+\nu)$, where E is the material property of Young's modulus and ν is the Poisson's ratio.

The authors quantified the model's ability to differentiate between tumor progression and radiation necrosis by doing an univariate analysis for the change in the longest dimension of the lesion in T1-weighted MR images (ROC AUC = 0.73), change in lesion volume (ROC AUC = 0.61) and FLAIR/T1 lesion quotient (ROC AUC = 0.55). Also, they did

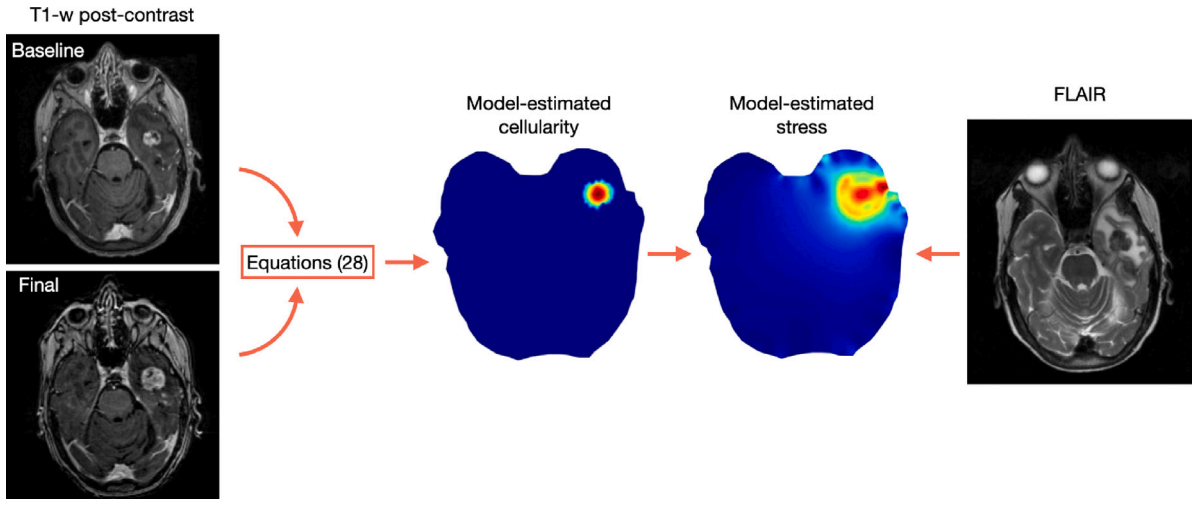

Fig. 7. Schematic of the biophysical model used in [84] for prediction of radiation necrosis and tumor progression by using MR T1-weighted and FLAIR images.
Source: Figure adapted from [84].

a radiomic analysis of 1080 radiomics features per patient with a ROC AUC of 0.82 and 0.77, depending on the training/validation dataset subsampling.

The study highlighted the successful differentiation of radiation necrosis from tumor progression using an imaging-driven biophysical model, even prior to pathological confirmation. This mechanism-based modeling method proved to be more effective than standard radiographic analysis, suggesting its potential as a robust tool for interpreting follow-up imaging.

5.3. The Von Bertalanffy model for the distinction between RN and progression

In an attempt to support clinicians in distinguishing between RN and progression, Ocaña-Tienda et al. [85] conducted a study using longitudinal data from patients after SRS. Their goal was to identify the growth dynamics of both conditions, with a particular focus on determining the growth exponents that best characterize progressive disease and RN events within the framework of the Von Bertalanffy model in Eq. (11).

The authors showed that growth exponents were the highest in the case of RN events. The median value of the growth exponent for progressive BMs following SRS ($n = 60$) was $\beta = 0.52$, contrasting with the median value of $\beta = 2.10$ observed for RN events ($n = 41$). This distinction proved to be statistically significant ($p < 0.001$), with an area under the ROC curve of 0.74. This finding supports using this variable as the basis for a classifier and may provide clinicians with an additional tool for effectively discerning between RN and tumor progression. The main advantage of this method is its reliance on T1-contrast MR images, which are routinely acquired in clinical practice, and the use of a very simple mathematical equation. In addition, the results obtained for the ROC AUC showed improvements over those previously obtained in univariate analyses [84].

5.4. A toy model of RN formation

The previously presented models are capable of fitting patient data and can serve as a tool for distinguishing between progression and RN. However, their primary focus is not on comprehending the underlying biology of the RN effect. Ocaña-Tienda et al. [86] developed a mathematical model to gain a better understanding of how RN events develop from a cellular point of view.

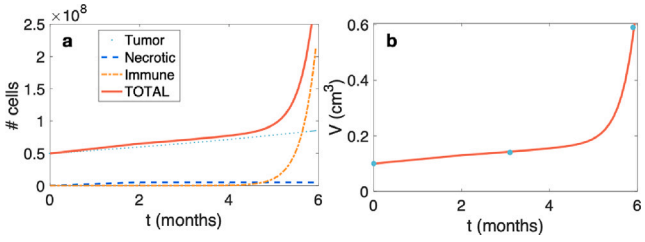

Fig. 8. Growth dynamics of a radiation necrosis event according to the model described by Eq. (30). **a.** Dynamics of each population (tumor, necrotic and immune cells) together with the total amount of cells over time **b.** Fitting curve to volumetric data from a patient diagnosed with radiation necrosis (blue points) using the mathematical model in Eq. (30) (continuous line).
Source: Figure adapted from [86].

The model accounts for three cell populations: tumor $T(t)$, necrotic $N(t)$ and immune cells $I(t)$, with dynamics given by

$$\frac{dT}{dt} = \rho T, \tag{30a}$$

$$\frac{dN}{dt} = H - \lambda_N I N, \tag{30b}$$

$$\frac{dI}{dt} = \gamma N + \theta I - \lambda_I I. \tag{30c}$$

Tumor cells were assumed to grow exponentially, with a growth rate ρ. The healthy cells surrounding the tumor that were killed by radiation were the source of necrotic cells, which was expressed mathematically as $H(t) = k \cdot \left(\tanh(t_N - t) + 1\right)/2$, where k represent the total number of healthy cells killed, which is proportional to the tumor's initial volume. Necrotic cells were cleared away by immune cells. Finally, the immune population appeared at a rate γ with the presence of necrosis, having a growth rate θ and a fixed death rate λ. Fig. 8 shows the three populations evolving on time (a) and a fitting to experimental data (b).

This straightforward model provides a reasonable explanation for the growth patterns observed in medical images during instances of RN. According to the mathematical model, this growth is consistent with the activity of the immune system, which is increased by the presence of a necrotic compartment of healthy cells killed by radiation. This model accurately captures the growth patterns observed in patient data, similar to the model proposed by León-Triana [83]. The main advantage of this model is its simplicity, characterized by a reduced number of parameters. However, it focuses exclusively on RN events and does not capture the behavior of other types of treatment responses.

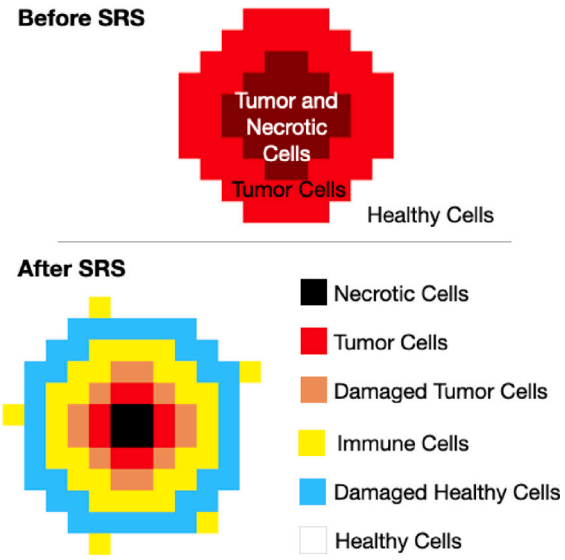

Fig. 9. Spatial distribution of cell populations before and after SRS. Different cellular populations may occupy each voxels, but the colors indicate the dominant population in each one.
Source: Figure adapted from [86].

5.5. A discrete stochastic simulator for response to SRS and RN classification

A discrete stochastic simulator was developed to better understand the dynamics of tumor growth and inflammatory response after SRS [86]. These models incorporate spatial and temporal detail, as well as critical biological processes such as cell division, death, and migration while minimizing computational cost [107].

Before treatment, it includes three cell populations: healthy, tumor, and necrotic, with probabilistic events for cell division, death, and migration. These events are defined by

$$P_{\text{Tdiv}} = \frac{\triangle x}{\tau_{\text{Tdiv}}}\left(1 - \frac{n_t + n_n + n_h}{K}\right), \tag{31a}$$

$$P_{\text{Tmig}} = \frac{\triangle x}{\tau_{\text{Tmig}}}\left(\frac{n_t + n_n + n_h}{K}\right), \tag{31b}$$

$$P_{\text{Tdeath}} = \frac{\triangle x}{\tau_{\text{Tdeath}}}\left(\tanh\left(\frac{10(n_t + n_n + n_h - K_{\text{act}})}{K}\right)\right), \tag{31c}$$

$$P_{\text{Hmig}} = \frac{\triangle x}{\tau_{\text{Hmig}}}\left(\tanh\left(\frac{10(n_t + n_n + n_h - 0.45K)}{K}\right)\right), \tag{31d}$$

with n_t, n_n, and n_h representing the total number of tumor, necrotic, and healthy cells in a voxel. The parameter τ determines the characteristic time of each process and K_{act}, the voxel carrying capacity.

To model the response to SRS, three additional populations were considered: immune cells, damaged tumor cells, and damaged healthy cells (Fig. 9), with event probabilities

$$P_{Ddie} = \frac{\triangle x}{k \cdot \tau_{\text{Trep}}}, \tag{32a}$$

$$P_{\text{Iact}} = \frac{\triangle x}{\tau_{\text{act}}} \cdot \frac{n_n}{n_i}\left(1 - \frac{n_t + n_n + n_h + n_d + n_{hd} + q \cdot n_i}{K}\right), \tag{32b}$$

$$P_{\text{Ikill}} = \frac{\triangle x}{\tau_{\text{kill}}} \cdot \frac{n_i}{n_n}\left(1 - \frac{n_t + n_n + n_h + n_d + n_{hd}}{K}\right), \tag{32c}$$

$$P_{\text{Ideath}} = \frac{\triangle x}{\tau_{\text{Ideath}}}, \tag{32d}$$

$$P_{\text{Imig}} = \frac{\triangle x}{\tau_{\text{Imig}}}\left(\frac{n_t + n_n + n_h + n_d + n_{hd} + q \cdot n_i}{K}\right). \tag{32e}$$

The effect of SRS was incorporated as a reduction in lesion volume, mathematically implemented as

$$S_f = S_{\hat{f}} \cdot \tanh\left(\frac{10(n_n - 0.45K)}{K}\right), \tag{33}$$

where $S_{\hat{f}}$ is the maximum survival fraction. The probability of lesion recurrence or radiation necrosis after SRS is influenced by the degree of damage to healthy cells. Authors also used the stochastic simulator to assess the model's ability to distinguish between recurrent lesions and RN events, obtaining a 97% accuracy (AUC = 0.97).

Through the use of a stochastic mesoscale simulator, this study provides a detailed representation of the interactions occurring within BMs. The effectiveness of the simulator was validated in distinguishing between recurrent lesions and RN events, supporting the utility of the growth exponent β in this differentiation [85].

5.6. Summary of radiation necrosis models

In the field of mathematical models for RN after SRS, several approaches offer valuable insights to distinguish RN from tumor progression and to understand the underlying biological processes. Dohm et al. [103] presented a biophysical model using MR T1-weighted and FLAIR images. They performed univariate analysis using change in longest dimension of the lesion, change in lesion volume, or FLAIR/T1 lesion quotient, and improved their classification accuracy by incorporating radiomic features into their model. Ocaña-Tienda et al. [85] relied solely on the growth exponent extracted from the volume at three time points as a classifier. This method proved to be the most straightforward way to discriminate RN from tumor progression and showed superior classification performance compared to the univariate analysis performed by Dohm et al. The other models helped to better understand the underlying process of radiation necrosis. León-Triana et al. [83] introduced a compartmental model and provided a mathematical basis for distinguishing between RN and true progression. Ocaña-Tienda et al. [86] proposed a toy model that biologically describes RN in the simplest way, and a stochastic simulator that provides a more comprehensive understanding of the dynamics by incorporating spatial and temporal details.

6. Discussion and future challenges

Despite the relevance of brain metastases and the historical interest in the development of mathematical models of primary brain tumors, the mathematical study of secondary brain tumors has been very scarce. This review aims to build a foundation for the expansion of further modeling work in the field of brain metastases.

We reviewed here the various mathematical modeling approaches that have been used to gain insight into the formation and growth of brain metastases (BMs). These modeling efforts encompass various biological mechanisms, including cell behavior such as proliferation, migration, and death, as well as cell interactions with primary tumors and other cell types and the effect of different treatments.

The two models reviewed that addressed the mechanisms behind the formation of BMs [71,73] approached the problem from the perspective of cells exiting a primary tumor. Subsequently, once they reach a secondary site, these cells undergo growth following Gompertzian dynamics. However, a number of studies have shown that the majority of cancer cells that succeed in crossing the blood–brain barrier (BBB) undergo cell death [6,10]. Those cells that manage to survive remain in close contact with blood vessels via vascular co-option [7]. Given that this scenario involves isolated cells interacting with their environment, a discrete mathematical model could be a practical approach. Such a model may be an effective way to illustrate how cells in the brain gradually evolve until they become a metastasis.

Given the scarce availability of data regarding the natural growth of BMs, the use of growth rates was employed in four of the reviewed

studies [74–77]. Notably, the first three studies computed the growth rate using a linear approximation, whereas the fourth one used an exponential equation. Although both Yoo et al. and Kobets et al. did not identify statistically significant differences in growth rates across various study variables such as tumor type, cancer stage, and chemotherapy use, Garcia et al. found that melanoma tumors exhibited a higher growth rate compared to other tumor types. Additionally, Shin et al. determined that the growth rate parameter had prognostic value. However, further research is required because some of the cited studies relied on measurements from only one time point, typically on diagnosis, and made assumptions about the second one, typically pre-diagnostic.

The remaining two studies focused on investigating untreated BMs [79,80] and approached the subject from different perspectives. Ocaña-Tienda et al. conducted the analysis using a dataset of patients having three distinct time points for untreated BMs and used the von Bertalanffy equation to compute the growth exponent. Remarkably, their findings unveiled that the natural growth of BMs is characterized by growth exponents larger than 1, where 1 corresponds to exponential growth dynamics. However, the study was based on a limited number of lesions, and it would be valuable to investigate the result in a larger dataset. On the other hand, Watanabe et al. proposed a mathematical model characterized by a tumor growth rate that decreases over time as tumor size increases, which does not match the experimental evidence of other works [78,79]. This dynamic resulted in the emergence of Gompertzian growth patterns.

As to the response to treatment, three out of the five reviewed studies [80,81,83] developed models to study the response of BMs to stereotactic radiotherapy (SRS). The study by Ocaña-Tienda et al. [79] characterized the growth of BMs after irradiation, chemotherapy, and combined treatment using three consecutive time points, finding that in terms of growth exponent, there were no differences between treatments. This finding was interpreted as a reduction in the heterogeneity of the tumor caused by all types of treatments regardless of their effectiveness. The study conducted by Butner et al. [82] introduced the response to immunotherapy, a promising treatment option for patients with BMs [108,109]. Their model demonstrated the potential to personalize immunotherapy treatments, enhancing the response for individual patients.

Tumor progression and radiation necrosis (RN) events present similar features on medical images, making it a challenge for clinicians to differentiate between them without using invasive techniques. This distinction is critical because the therapeutic approaches for these two conditions are completely different. Given the challenges associated with RN following SRS, mathematicians have worked to develop various models aimed at understanding the complex RN process and effectively distinguishing it from true tumor progression. These models include two ordinary differential equation (ODE) models, a biophysical model, a discrete stochastic simulator, and the use of the growth exponent derived from the von Bertalanfy equation. The findings from these reviewed studies underscore the potential of mathematical models as valuable tools in tackling the crucial challenge of distinguishing between disease progression and radiation necrosis (RN). However, there remains room for improvement in achieving higher accuracy. Notably, in the univariate analyses conducted by Dohm et al. [84], which encompassed parameters such as the longest dimension of the lesion, changes in volume, and FLAIR/T1 lesion quotient, the area under the ROC curve did not exceed 0.75. Similarly, Ocaña-Tienda et al. [85] achieved an area under the ROC curve of 0.74 using growth exponents. While these results are promising, further refinement is needed to enhance the accuracy of these models in clinical practice.

Surgery, either alone or in combination with radiation therapy, is another treatment of choice for selected BM patients [1,110]. Resection has been mathematically modeled in the case of gliomas [111–114], but the authors are not aware of any article in which this treatment has been mathematically described for BMs.

Radiomic studies have demonstrated enhanced classification capabilities, but they demand substantial amounts of data to ensure credible results and prevent overfitting. This is particularly critical in the case of BMs, given their broad range of characteristics resulting from diverse locations, primary tumor types, and varying sizes and shapes. Consequently, mechanistic models are likely to outperform radiomics in this scenario where data availability is limited. However, it is worth noting that recently, several publicly accessible databases with annotated BMs have emerged [115–117], increasing the feasibility and accessibility of BM research to other research groups both using AI and mechanistic mathematical models.

Notably, many of the reviewed studies were published in biomedical or multidisciplinary journals and involved clinician co-authors and simple mathematical modeling approaches. This highlights the practical interest of mathematical models in managing BM patients. Validating these models with additional clinical and experimental data remains a crucial step in utilizing them as clinical tools aiding in the decision-making process.

Significant distinctions between BMs and other types of metastases, as well as the disparities between BMs and glioblastoma, emphasize the critical importance of understanding the unique nature of BMs. Despite the objective high impact of this devastating illness, it is surprising to note that the mathematical community has shown a limited interest in investigating and modeling BMs. All of the studies based on clinical data considered were retrospective using available data. In the future, large-scale retrospective and prospective studies will be crucial to validate the value of the results already obtained and develop improved mathematical models addressing the problems considered here and many others. The integration of experimental, mathematical, and computational approaches holds great promise for addressing unresolved questions about BM development. By gaining a deeper understanding of the BM formation process, targeted therapies may be developed to prevent its occurrence at different stages. Such advances in the field require close interdisciplinary collaboration between mathematicians and biomedical experts to promote the development of more accurate models. This synergy fosters the creation of increasingly practical models, thereby enhancing the feasibility of advancing brain metastases research and improving patient care.

CRediT authorship contribution statement

Beatriz Ocaña-Tienda: Conceptualization, Formal analysis, Investigation, Methodology, Resources, Software, Validation, Visualization, Writing – original draft, Writing – review & editing. **Víctor M. Pérez-García:** Conceptualization, Funding acquisition, Investigation, Methodology, Project administration, Resources, Supervision, Validation, Writing – review & editing.

Declaration of competing interest

All authors declare that they have no conflicts of interest.

Data availability

No data was used for the research described in the article.

Acknowledgments

This work was partially supported by project PDC2022-133520-I00 funded by Ministerio de Ciencia e Innovación/ Agencia Estatal de investigación (doi:10.13039/501100011033) and European Union "NextGenerationEU/PRTR", project SBPLY/21/180501/000145, funded by Junta de Comunidades de Castilla-La Mancha, Spain (and European Regional Development Fund (FEDER, EU), and partially supported by the Scientific Foundation of Asociación Española contra el Cáncer grant RENACER (coordinated projects AECC2023 grant ID PRYCO234528VALI). BOT is supported by Ministerio de Ciencia e Innovación, Spain (grant PRE2020-092178). The funders had no role in study design, data collection and analysis, decision to publish, or preparation of the manuscript.

References

[1] A. Lauko, Y. Rauf, M.S. Ahluwalia, Medical management of brain metastases, Neurooncol. Adv. 2 (1) (2020) vdaa015, http://dx.doi.org/10.1093/noajnl/vdaa015.

[2] M.J. Moravan, P.E. Fecci, C.K. Anders, et al., Current multidisciplinary management of brain metastases, Cancer 126 (7) (2020) 1390–1406, http://dx.doi.org/10.1002/cncr.32714.

[3] Y. Tsukada, A. Fouad, J.W. Pickren, W.W. Lane, Central nervous system metastasis from breast carcinoma. Autopsy study, Cancer 52 (12) (1983) 2349–2354.

[4] A.A. Aizer, N. Lamba, M.S. Ahluwalia, et al., Brain metastases: A Society for Neuro-Oncology (SNO) consensus review on current management and future directions, Neuro Oncol. 24 (10) (2022) 1613–1646, http://dx.doi.org/10.1093/neuonc/noac118.

[5] L. Nayak, E.Q. Lee, P.Y. Wen, Epidemiology of brain metastases, Curr. Oncol. Rep. 14 (1) (2012) 48–54, http://dx.doi.org/10.1007/s11912-011-0203-y.

[6] Y. Kienast, L. von Baumgarten, M. Fuhrmann, et al., Real-time imaging reveals the single steps of brain metastasis formation, Nature Med. 16 (1) (2010) 116–122, http://dx.doi.org/10.1038/nm.2072.

[7] P. García-Gómez, M. Valiente, Vascular co-option in brain metastasis, Angiogenesis 23 (1) (2020) 3–8, http://dx.doi.org/10.1007/s10456-019-09693-x.

[8] J. Massagué, A.C. Obenauf, Metastatic colonization by circulating tumour cells, Nature 529 (7586) (2016) 298–306, http://dx.doi.org/10.1038/nature17038.

[9] M. Lorger, B. Felding-Habermann, Capturing changes in the brain microenvironment during initial steps of breast cancer brain metastasis, Am. J. Pathol. 176 (6) (2010) 2958–2971, http://dx.doi.org/10.2353/ajpath.2010.090838.

[10] F. Winkler, The brain metastatic niche, J. Mol. Med. 93 (11) (2015) 1213–1220, http://dx.doi.org/10.1007/s00109-015-1357-0.

[11] A.S. Berghoff, Y. Liao, M.A. Karreman, et al., Identification and characterization of cancer cells that initiate metastases to the brain and other organs, Mol. Cancer Res. 19 (4) (2021) 688–701, http://dx.doi.org/10.1158/1541-7786.MCR-20-0863.

[12] S. Valastyan, R.A. Weinberg, Tumor metastasis: molecular insights and evolving paradigms, Cell 147 (2) (2011) 275–292, http://dx.doi.org/10.1016/j.cell.2011.09.024.

[13] S. Vanharanta, J. Massagué, Origins of metastatic traits, Cancer Cell 24 (4) (2013) 410–421, http://dx.doi.org/10.1016/j.ccr.2013.09.007.

[14] M. Kuznetsov, J. Clairambault, V. Volpert, Improving cancer treatments via dynamical biophysical models, Phys. Life Rev. 39 (2021) 1–48, http://dx.doi.org/10.1016/j.plrev.2021.10.001.

[15] F. Michor, K. Beal, Improving cancer treatment via mathematical modeling: Surmounting the challenges is worth the effort, Cell 163 (5) (2015) 1059–1063, http://dx.doi.org/10.1016/j.cell.2015.11.002.

[16] M. Sturrock, W. Hao, J. Schwartzbaum, G.A. Rempala, A mathematical model of pre-diagnostic glioma growth, J. Theoret. Biol. 380 (2015) 299–308, http://dx.doi.org/10.1016/j.jtbi.2015.06.003.

[17] K.P. Slavkova, S.H. Patel, Z. Cacini, et al., Mathematical modelling of the dynamics of image-informed tumor habitats in a murine model of glioma, Sci. Rep. 13 (1) (2023) 2916, http://dx.doi.org/10.1038/s41598-023-30010-6.

[18] S. Khajanchi, The impact of immunotherapy on a glioma immune interaction model, Chaos Solitons Fractals 152 (1) (2021) 111346, http://dx.doi.org/10.1016/j.chaos.2021.111346.

[19] K.R. Swanson, R.C. Rockne, J. Claridge, M.A. Chaplain, E.C. Alvord Jr., A.R. Anderson, Quantifying the role of angiogenesis in malignant progression of gliomas: in silico modeling integrates imaging and histology, Cancer Res. 71 (24) (2011) 7366–7375, http://dx.doi.org/10.1158/0008-5472.CAN-11-1399.

[20] P. Gerlee, S. Nelander, Travelling wave analysis of a mathematical model of glioblastoma growth, Math. Biosci. 276 (1) (2016) 75–81, http://dx.doi.org/10.1016/j.mbs.2016.03.004.

[21] S. Stein, R. Zhao, H. Haeno, I. Vivanco, F. Michor, Mathematical modeling identifies optimum lapatinib dosing schedules for the treatment of glioblastoma patients, PLoS Comput. Biol. 14 (1) (2018) e1005924, http://dx.doi.org/10.1371/journal.pcbi.1005924.

[22] Z. Ma, B. Niu, T.A. Phan, et al., Stochastic growth pattern of untreated human glioblastomas predicts the survival time for patients, Sci. Rep. 10 (1) (2020) 6642, http://dx.doi.org/10.1038/s41598-020-63394-w.

[23] M. Aubert, M. Badoual, S. Féreol, C. Christov, B. Grammaticos, A cellular automaton model for the migration of glioma cells, Phys. Biol. 3 (2) (2006) 93–100, http://dx.doi.org/10.1088/1478-3975/3/2/001.

[24] H. Hatzikirou, D. Basanta, M. Simon, K. Schaller, A. Deutsch, 'Go or grow': the key to the emergence of invasion in tumour progression? Math. Med. Biol. 29 (1) (2012) 49–65, http://dx.doi.org/10.1093/imammb/dqq011.

[25] M. Tektonidis, H. Hatzikirou, A. Chauvière, M. Simon, K. Schaller, A. Deutsch, Identification of intrinsic in vitro cellular mechanisms for glioma invasion, J. Theoret. Biol. 287 (2011) 131–147, http://dx.doi.org/10.1016/j.jtbi.2011.07.012.

[26] D. Basanta, M. Simon, H. Hatzikirou, A. Deutsch, Evolutionary game theory elucidates the role of glycolysis in glioma progression and invasion, Cell Prolif. 41 (6) (2008) 980–987, http://dx.doi.org/10.1111/j.1365-2184.2008.00563.x.

[27] N.G. Burnet, R. Jena, S.J. Jefferies, S.P. Stenning, N.F. Kirkby, Mathematical modelling of survival of glioblastoma patients suggests a role for radiotherapy dose escalation and predicts poorer outcome after delay to start treatment, Clin. Oncol. (R. Coll. Radiol.) 18 (2) (2006) 93–103, http://dx.doi.org/10.1016/j.clon.2005.08.017.

[28] N.F. Kirkby, S.J. Jefferies, R. Jena, N.G. Burnet, A mathematical model of the treatment and survival of patients with high-grade brain tumours, J. Theoret. Biol. 245 (1) (2007) 112–124, http://dx.doi.org/10.1016/j.jtbi.2006.09.007.

[29] R. Rockne, E.C. Alvord Jr., J.K. Rockhill, K.R. Swanson, A mathematical model for brain tumor response to radiation therapy, J. Math. Biol. 58 (4–5) (2009) 561–578, http://dx.doi.org/10.1007/s00285-008-0219-6.

[30] C. Faivre, D. Barbolosi, E. Pasquier, N. André, A mathematical model for the administration of temozolomide: comparative analysis of conventional and metronomic chemotherapy regimens, Cancer Chemother. Pharmacol. 71 (4) (2013) 1013–1019, http://dx.doi.org/10.1007/s00280-013-2095-z.

[31] D. Corwin, C. Holdsworth, R.C. Rockne, et al., Toward patient-specific, biologically optimized radiation therapy plans for the treatment of glioblastoma, PLoS One 8 (11) (2013) e79115, http://dx.doi.org/10.1371/journal.pone.0079115.

[32] K. Leder, K. Pitter, Q. LaPlant, et al., Mathematical modeling of PDGF-driven glioblastoma reveals optimized radiation dosing schedules, Cell 156 (3) (2014) 603–616, http://dx.doi.org/10.1016/j.cell.2013.12.029.

[33] K.C. Iarosz, F.S. Borges, A.M. Batista, et al., Mathematical model of brain tumour with glia-neuron interactions and chemotherapy treatment, J. Theoret. Biol. 368 (2015) 113–121, http://dx.doi.org/10.1016/j.jtbi.2015.01.006.

[34] H. Badri, K. Pitter, E.C. Holland, F. Michor, K. Leder, Optimization of radiation dosing schedules for proneural glioblastoma, J. Math. Biol. 72 (5) (2016) 1301–1336, http://dx.doi.org/10.1007/s00285-015-0908-x.

[35] H. Yan, M. Romero-López, L.I. Benitez, et al., 3D mathematical modeling of glioblastoma suggests that transdifferentiated vascular endothelial cells mediate resistance to current standard-of-care therapy, Cancer Res. 77 (15) (2017) 4171–4184, http://dx.doi.org/10.1158/0008-5472.CAN-16-3094.

[36] E. Fernandez-Cara, J. Limaco, L. Prouvée, Optimal control of a two-equation model of radiotherapy, Math. Control Relat. Fields 8 (1) (2018) 117–133, http://dx.doi.org/10.3934/mcrf.2018005.

[37] J. Trobia, K. Tian, A.M. Batista, et al., Mathematical model of brain tumor growth with drug resistance, Commun. Nonlinear Sci. Numer. Simul. 103 (1) (2021) 106013, http://dx.doi.org/10.1016/j.cnsns.2021.106013.

[38] D.A. Hormuth II, K.A. Al Feghali, A.M. Elliott, T.E. Yankeelov, C. Chung, Image-based personalization of computational models for predicting response of high-grade glioma to chemoradiation, Sci. Rep. 11 (1) (2021) 8520.

[39] E. Scribner, O. Saut, P. Province, A. Bag, T. Colin, H.M. Fathallah-Shaykh, Effects of anti-angiogenesis on glioblastoma growth and migration: model to clinical predictions, PLoS One 9 (12) (2014) e115018, http://dx.doi.org/10.1371/journal.pone.0115018.

[40] O. Saut, J.B. Lagaert, T. Colin, H.M. Fathallah-Shaykh, A multilayer grow-or-go model for GBM: effects of invasive cells and anti-angiogenesis on growth, Bull. Math. Biol. 76 (9) (2014) 2306–2333, http://dx.doi.org/10.1007/s11538-014-0007-y.

[41] S.C. Massey, H. White, P. Whitmire, et al., Image-based metric of invasiveness predicts response to adjuvant temozolomide for primary glioblastoma, PLoS One 15 (3) (2020) e0230492, http://dx.doi.org/10.1371/journal.pone.0230492.

[42] J.J. Bosque, G.F. Calvo, V.M. Pérez-García, M.C. Navarro, The interplay of blood flow and temperature in regional hyperthermia: a mathematical approach, R. Soc. Open Sci. 8 (1) (2021) 201234, http://dx.doi.org/10.1098/rsos.201234.

[43] M. Conte, Y. Dzierma, S. Knobe, C. Surulescu, Mathematical modeling of glioma invasion and therapy approaches via kinetic theory of active particles, Math. Models Methods Appl. Sci. 33 (5) (2023) 1009–1051, http://dx.doi.org/10.1142/S0218202523500227.

[44] H. Yan, M. Romero-López, L.I. Benitez, et al., 3D mathematical modeling of glioblastoma suggests that transdifferentiated vascular endothelial cells mediate resistance to current standard-of-care therapy, Cancer Res. 77 (15) (2017) 4171–4184, http://dx.doi.org/10.1158/0008-5472.CAN-16-3094.

[45] I.C. Sorribes, S.K. Handelman, H.V. Jain, Mitigating temozolomide resistance in glioblastoma via DNA damage-repair inhibition, J. R. Soc. Interface 17 (162) (2020) 20190722, http://dx.doi.org/10.1098/rsif.2019.0722.

[46] M. Rabé, S. Dumont, A. Álvarez-Arenas, et al., Identification of a transient state during the acquisition of temozolomide resistance in glioblastoma, Cell Death Dis. 11 (1) (2020) 19, http://dx.doi.org/10.1038/s41419-019-2200-2.

[47] M. Minata, A. Audia, J. Shi, et al., Phenotypic plasticity of invasive edge glioma stem-like cells in response to ionizing radiation, Cell Rep. 26 (7) (2019) 1893–1905, http://dx.doi.org/10.1016/j.celrep.2019.01.076, e7.

[48] B. Segura-Collar, J. Jiménez-Sánchez, R. Gargini, et al., On optimal temozolomide scheduling for slowly growing glioblastomas, Neurooncol. Adv. 4 (1) (2022) vdac155, http://dx.doi.org/10.1093/noajnl/vdac155.

[49] G.L. Celora, H.M. Byrne, C.E. Zois, P.G. Kevrekidis, Phenotypic variation modulates the growth dynamics and response to radiotherapy of solid tumours under normoxia and hypoxia, J. Theoret. Biol. 527 (2021) 110792, http://dx.doi.org/10.1016/j.jtbi.2021.110792.

[50] K.R. Swanson, H.L. Harpold, D.L. Peacock, et al., Velocity of radial expansion of contrast-enhancing gliomas and the effectiveness of radiotherapy in individual patients: a proof of principle, Clin. Oncol. (R. Coll. Radiol.) 20 (4) (2008) 301–308, http://dx.doi.org/10.1016/j.clon.2008.01.006.

[51] C.H. Wang, J.K. Rockhill, M. Mrugala, et al., Prognostic significance of growth kinetics in newly diagnosed glioblastomas revealed by combining serial imaging with a novel biomathematical model, Cancer Res. 69 (23) (2009) 9133–9140, http://dx.doi.org/10.1158/0008-5472.CAN-08-3863.

[52] J. Pérez-Beteta, D. Molina-García, J.A. Ortiz-Alhambra, et al., Tumor surface regularity at MR imaging predicts survival and response to surgery in patients with glioblastoma, Radiology 288 (1) (2018) 218–225, http://dx.doi.org/10.1148/radiol.2018171051.

[53] J. Pérez-Beteta, D. Molina-García, M. Villena, et al., Morphologic features on MR imaging classify multifocal glioblastomas in different prognostic groups, AJNR Am. J. Neuroradiol. 40 (4) (2019) 634–640, http://dx.doi.org/10.3174/ajnr.A6019.

[54] S. Urcun, D. Baroli, P.Y. Rohan, W. Skalli, V. Lubrano, S.P. Bordas, G. Sciume, Non-operable glioblastoma: proposition of patient-specific forecasting by image-informed poromechanical model, Brain Multiph. 4 (2023) 100067, http://dx.doi.org/10.1016/j.brain.2023.100067.

[55] D. Barbolosi, A. Benabdallah, F. Hubert, F. Verga, Mathematical and numerical analysis for a model of growing metastatic tumors, Math. Biosci. 218 (1) (2009) 1–14, http://dx.doi.org/10.1016/j.mbs.2008.11.008.

[56] N. Hartung, S. Mollard, D. Barbolosi, et al., Mathematical modeling of tumor growth and metastatic spreading: validation in tumor-bearing mice, Cancer Res. 74 (22) (2014) 6397–6407, http://dx.doi.org/10.1158/0008-5472.CAN-14-0721.

[57] S. Benzekry, A. Tracz, M. Mastri, R. Corbelli, D. Barbolosi, J.M. Ebos, Modeling spontaneous metastasis following surgery: An in vivo-in silico approach, Cancer Res. 76 (3) (2016) 535–547, http://dx.doi.org/10.1158/0008-5472.CAN-15-1389.

[58] L.C. Franssen, T. Lorenzi, A.E.F. Burgess, M.A.J. Chaplain, A mathematical framework for modelling the metastatic spread of cancer, Bull. Math. Biol. 81 (6) (2019) 1965–2010, http://dx.doi.org/10.1007/s11538-019-00597-x.

[59] A.R.A. Anderson, M.A.J. Chaplain, E.L. Newman, R.J.C. Steele, A.M. Thompson, Mathematical modelling of tumour invasion and metastasis, J. Theor. Med. 2 (1) (2000) 490902, http://dx.doi.org/10.1080/10273660008833042.

[60] G.W. Brodland, J.H. Veldhuis, The mechanics of metastasis: insights from a computational model, PLoS One 7 (9) (2012) e44281, http://dx.doi.org/10.1371/journal.pone.0044281.

[61] I. Ramis-Conde, D. Drasdo, A.R. Anderson, M.A. Chaplain, Modeling the influence of the E-cadherin-beta-catenin pathway in cancer cell invasion: a multiscale approach, Biophys. J. 95 (1) (2008) 155–165, http://dx.doi.org/10.1529/biophysj.107.114678.

[62] I. Ramis-Conde, M.A. Chaplain, A.R. Anderson, D. Drasdo, Multi-scale modelling of cancer cell intravasation: the role of cadherins in metastasis, Phys. Biol. 6 (1) (2009) 016008, http://dx.doi.org/10.1088/1478-3975/6/1/016008.

[63] A. Mujoomdar, J.H. Austin, R. Malhotra, et al., Clinical predictors of metastatic disease to the brain from non-small cell lung carcinoma: primary tumor size, cell type, and lymph node metastases, Radiology 242 (3) (2007) 882–888, http://dx.doi.org/10.1148/radiol.2423051707.

[64] D. Diego, G.F. Calvo, V.M. Pérez-García, Modeling the connection between primary and metastatic tumors, J. Math. Biol. 67 (3) (2013) 657–692, http://dx.doi.org/10.1007/s00285-012-0565-2.

[65] A. Álvarez-Arenas, W. Souleyreau, A. Emanuelli, et al., Practical identifiability analysis of a mechanistic model for the time to distant metastatic relapse and its application to renal cell carcinoma, PLoS Comput. Biol. 18 (8) (2022) e1010444, http://dx.doi.org/10.1371/journal.pcbi.1010444.

[66] C. Bigarré, F. Bertucci, P. Finetti, G. Macgrogan, X. Muracciole, S. Benzekry, Mechanistic modeling of metastatic relapse in early breast cancer to investigate the biological impact of prognostic biomarkers, Comput. Methods Programs Biomed. 231 (2023) 107401, http://dx.doi.org/10.1016/j.cmpb.2023.107401.

[67] I.M. Bulai, M.C. De Bonis, C. Laurita, V. Sagaria, Modeling metastatic tumor evolution, numerical resolution and growth prediction, Math. Comput. Simulation 203 (2023) 721–740, http://dx.doi.org/10.1016/j.matcom.2022.07.002.

[68] A. Camacho, S. Jerez, Bone metastasis treatment modeling via optimal control, J. Math. Biol. 78 (1–2) (2019) 497–526, http://dx.doi.org/10.1007/s00285-018-1281-3.

[69] D. Barbolosi, I. Summer, C. Meille, et al., Modeling therapeutic response to radioiodine in metastatic thyroid cancer: a proof-of-concept study for individualized medicine, Oncotarget 8 (24) (2017) 39167–39176, http://dx.doi.org/10.18632/oncotarget.16637.

[70] H. Peng, H. Tan, W. Zhao, et al., Computational systems biology in cancer brain metastasis, Front. Biosci. 8 (1) (2016) 169–186, http://dx.doi.org/10.2741/s456.

[71] M. Bilous, C. Serdjebi, A. Boyer, et al., Quantitative mathematical modeling of clinical brain metastasis dynamics in non-small cell lung cancer, Sci. Rep. 9 (1) (2019) 13018, http://dx.doi.org/10.1038/s41598-019-49407-3.

[72] S. Benzekry, P. Schlicke, A. Mogenet, L. Greillier, P. Tomasini, E. Simon, Computational markers for personalized prediction of outcomes in non-small cell lung cancer patients with brain metastases, Clin. Exp. Metastasis 41 (1) (2024) 55–68, http://dx.doi.org/10.1007/s10585-023-10245-3.

[73] D.L. Smith, B.G. Debeb, H.D. Thames, W.A. Woodward, Computational modeling of micrometastatic breast cancer radiation dose response, Int. J. Radiat. Oncol. Biol. Phys. 96 (1) (2016) 179–187, http://dx.doi.org/10.1016/j.ijrobp.2016.04.014.

[74] H. Yoo, E. Jung, B.H. Nam, et al., Growth rate of newly developed metastatic brain tumors after thoracotomy in patients with non-small cell lung cancer, Lung Cancer 71 (2) (2011) 205–208, http://dx.doi.org/10.1016/j.lungcan.2010.05.013.

[75] M.A. Garcia, M. Anwar, Y. Yu, et al., Brain metastasis growth on preradiosurgical magnetic resonance imaging, Pract. Radiat. Oncol. 8 (6) (2018) e369–e376, http://dx.doi.org/10.1016/j.prro.2018.06.004.

[76] A.J. Kobets, R. Backus, R. Fluss, A. Lee, P.A. Lasala, Evaluating the natural growth rate of metastatic cancer to the brain, Surg. Neurol. Int. 11 (1) (2020) 254, http://dx.doi.org/10.25259/SNI_291_2020.

[77] Y. Shin, J.S. Chang, Y. Kim, et al., Mathematical prediction with pretreatment growth rate of metastatic cancer on outcomes: implications for the characterization of oligometastatic disease, Front. Oncol. 13 (1) (2023) 1061881, http://dx.doi.org/10.3389/fonc.2023.1061881.

[78] V.M. Pérez-García, G.F. Calvo, J.J. Bosque, et al., Universal scaling laws rule explosive growth in human cancers, Nat. Phys. 16 (12) (2020) 1232–1237, http://dx.doi.org/10.1038/s41567-020-0978-6.

[79] B. Ocaña-Tienda, J. Pérez-Beteta, J. Jiménez-Sánchez, et al., Growth exponents reflect evolutionary processes and treatment response in Brain Metastases, NPJ Syst. Biol. Appl. 9 (1) (2023) 35, http://dx.doi.org/10.1038/s41540-023-00298-1.

[80] Y. Watanabe, E.L. Dahlman, K.Z. Leder, S.K. Hui, A mathematical model of tumor growth and its response to single irradiation, Theor. Biol. Med. Model. 13 (1) (2016) 6, http://dx.doi.org/10.1186/s12976-016-0032-7.

[81] S. Nawrocki, B. Zubik-Kowal, Clinical study and numerical simulation of brain cancer dynamics under radiotherapy, Commun. Nonlinear Sci. Numer. Simul. 22 (1) (2015) 564–573, http://dx.doi.org/10.1016/j.cnsns.2014.08.001.

[82] J.D. Butner, Z. Wang, D. Elganainy, et al., A mathematical model for the quantification of a patient's sensitivity to checkpoint inhibitors and long-term tumour burden, Nat. Biomed. Eng. 5 (4) (2021) 297–308, http://dx.doi.org/10.1038/s41551-020-00662-0.

[83] O. León-Triana, J. Pérez-Beteta, D. Albillo, et al., Brain Metastasis response to stereotactic radio surgery: A mathematical approach, Mathematics 9 (7) (2021) 716, http://dx.doi.org/10.3390/math9070716.

[84] A.E. Dohm, T.M. Nickles, C.E. Miller, et al., Clinical assessment of a biophysical model for distinguishing tumor progression from radiation necrosis, Med. Phys. 48 (7) (2021) 3852–3859, http://dx.doi.org/10.1002/mp.14999.

[85] B. Ocaña-Tienda, J. Pérez-Beteta, D. Molina-García, et al., Growth dynamics of brain metastases differentiate radiation necrosis from recurrence, Neurooncol. Adv. 5 (1) (2022) vdac179, http://dx.doi.org/10.1093/noajnl/vdac179.

[86] B. Ocaña-Tienda, O. León-Triana, J. Pérez-Beteta, J. Jiménez-Sánchez, V.M. Pérez-García, Radiation necrosis after radiation therapy treatment of brain metastases: A computational approach, PLoS Comput. Biol. 20 (1) (2024) e1011400, http://dx.doi.org/10.1371/journal.pcbi.1011400.

[87] K. Iwata, K. Kawasaki, N. Shigesada, A dynamical model for the growth and size distribution of multiple metastatic tumors, J. Theoret. Biol. 203 (2) (2000) 177–186, http://dx.doi.org/10.1006/jtbi.2000.1075.

[88] N.U. Lin, E.Q. Lee, H. Aoyama, et al., Response assessment criteria for brain metastases: proposal from the RANO group, Lancet Oncol. 16 (6) (2015) e270–e278, http://dx.doi.org/10.1016/S1470-2045(15)70057-4.

[89] J.M. Qian, A. Mahajan, J.B. Yu, et al., Comparing available criteria for measuring brain metastasis response to immunotherapy, J. Neurooncol. 132 (3) (2017) 479–485, http://dx.doi.org/10.1007/s11060-017-2398-8.

[90] L. Von Bertalanffy, Quantitative laws in metabolism and growth, Q. Rev. Biol. 32 (3) (1957) 217–231, http://dx.doi.org/10.1086/401873.

[91] R.A. Patchell, P.A. Tibbs, J.W. Walsh, et al., A randomized trial of surgery in the treatment of single metastases to the brain, N. Engl. J. Med. 322 (8) (1990) 494–500, http://dx.doi.org/10.1056/NEJM199002223220802.

[92] D.W. Andrews, C.B. Scott, P.W. Sperduto, et al., Whole brain radiation therapy with or without stereotactic radiosurgery boost for patients with one to three brain metastases: phase III results of the RTOG 9508 randomised trial, Lancet 363 (9422) (2004) 1665–1672, http://dx.doi.org/10.1016/S0140-6736(04)16250-8.

[93] J.Z. Wang, Z. Huang, S.S. Lo, W.T. Yuh, N.A. Mayr, A generalized linear-quadratic model for radiosurgery, stereotactic body radiation therapy, and high-dose rate brachytherapy, Sci. Transl. Med. 2 (39) (2010) 39ra48, http://dx.doi.org/10.1126/scitranslmed.3000864.

[94] V.M. Pérez-García, L.E. Ayala-Hernández, J. Belmonte-Beitia, et al., Computational design of improved standardized chemotherapy protocols for grade II oligodendrogliomas, PLoS Comput. Biol. 15 (7) (2019) e1006778, http://dx.doi.org/10.1371/journal.pcbi.1006778.

[95] G. Lorenzo, N. di Muzio, C.L. Deantoni, et al., Patient-specific forecasting of postradiotherapy prostate-specific antigen kinetics enables early prediction of biochemical relapse, iScience 25 (11) (2022) 105430, http://dx.doi.org/10.1016/j.isci.2022.105430.

[96] F. Cicone, L. Carideo, C. Scaringi, et al., Long-term metabolic evolution of brain metastases with suspected radiation necrosis following stereotactic radiosurgery: longitudinal assessment by F-DOPA PET, Neuro Oncol. 23 (6) (2021) 1024–1034, http://dx.doi.org/10.1093/neuonc/noaa239.

[97] S. Miyatake, N. Nonoguchi, M. Furuse, et al., Patho-physiology, diagnosis, and treatment of radiation necrosis in the brain, Neurol. Med. Chir. 55 (1) (2015) 50–59, http://dx.doi.org/10.2176/nmc.ra.2014-0188.

[98] Z.A. Kohutek, Y. Yamada, T.A. Chan, et al., Long-term risk of radionecrosis and imaging changes after stereotactic radiosurgery for brain metastases, J. Neurooncol. 125 (1) (2015) 149–156, http://dx.doi.org/10.1007/s11060-015-1881-3.

[99] G. Minniti, E. Clarke, G. Lanzetta, et al., Stereotactic radiosurgery for brain metastases: analysis of outcome and risk of brain radionecrosis, Radiat. Oncol. 6 (1) (2011) 48, http://dx.doi.org/10.1186/1748-717X-6-48.

[100] N. Verma, M.C. Cowperthwaite, M.G. Burnett, M.K. Markey, Differentiating tumor recurrence from treatment necrosis: A review of neuro-oncologic imaging strategies, Neuro Oncol. 15 (5) (2013) 515–534, http://dx.doi.org/10.1093/neuonc/nos307.

[101] M. Ammirati, C.S. Cobbs, M.E. Linskey, et al., The role of retreatment in the management of recurrent/progressive brain metastases: a systematic review and evidence-based clinical practice guideline, J. Neurooncol. 96 (1) (2010) 85–96, http://dx.doi.org/10.1007/s11060-009-0055-6.

[102] J.H. Suh, R. Kotecha, S.T. Chao, M.S. Ahluwalia, A. Sahgal, E.L. Chang, Current approaches to the management of brain metastases, Nat. Rev. Clin. Oncol. 17 (5) (2020) 279–299, http://dx.doi.org/10.1038/s41571-019-0320-3.

[103] S. Narasimhan, H.B. Johnson, T.M. Nickles, et al., Biophysical model-based parameters to classify tumor recurrence from radiation-induced necrosis for brain metastases, Med. Phys. 46 (5) (2019) 2487–2496, http://dx.doi.org/10.1002/mp.13461.

[104] J.A. Weis, M.I. Miga, L.R. Arlinghaus, et al., A mechanically coupled reaction–diffusion model for predicting the response of breast tumors to neoadjuvant chemotherapy, Phys. Med. Biol. 58 (17) (2013) 5851–5866, http://dx.doi.org/10.1088/0031-9155/58/17/5851.

[105] J.A. Weis, M.I. Miga, L.R. Arlinghaus, et al., Predicting the response of breast cancer to neoadjuvant therapy using a mechanically coupled reaction-diffusion model, Cancer Res. 75 (22) (2015) 4697–4707, http://dx.doi.org/10.1158/0008-5472.CAN-14-2945.

[106] J.A. Weis, M.I. Miga, T.E. Yankeelov, Three-dimensional image-based mechanical modeling for predicting the response of breast cancer to neoadjuvant therapy, Comput. Methods Appl. Mech. Engrg. 314 (2017) 494–512, http://dx.doi.org/10.1016/j.cma.2016.08.024.

[107] J. Jiménez-Sánchez, Á. Martínez-Rubio, A. Popov, et al., A mesoscopic simulator to uncover heterogeneity and evolutionary dynamics in tumors, PLoS Comput. Biol. 17 (2) (2021) e1008266, http://dx.doi.org/10.1371/journal.pcbi.1008266.

[108] P.K. Brastianos, S.L. Carter, S. Santagata, et al., Genomic characterization of brain metastases reveals branched evolution and potential therapeutic targets, Cancer Discov. 5 (11) (2015) 1164–1177, http://dx.doi.org/10.1158/2159-8290.CD-15-0369.

[109] H.A. Tawbi, P.A. Forsyth, A. Algazi, et al., Combined nivolumab and ipilimumab in melanoma metastatic to the brain, N. Engl. J. Med. 379 (8) (2018) 722–730, http://dx.doi.org/10.1056/NEJMoa1805453.

[110] C.I. Ene, S.D. Ferguson, Surgical management of brain metastasis: Challenges and nuances, Front. Oncol. 12 (2022) 847110, http://dx.doi.org/10.3389/fonc.2022.847110.

[111] D.E. Woodward, J. Cook, P. Tracqui, G.C. Gruywagen, J.D. Murray, E.C. Alvord Jr., A mathematical model of glioma growth: the effect of extent of surgical resection, Cell Prolif. 29 (6) (1996) 269–288, http://dx.doi.org/10.1111/j.1365-2184.1996.tb01580.x.

[112] K.R. Swanson, R.C. Rostomily, E.C. Alvord Jr., A mathematical modelling tool for predicting survival of individual patients following resection of glioblastoma: a proof of principle, Br. J. Cancer 98 (1) (2008) 113–119, http://dx.doi.org/10.1038/sj.bjc.6604125.

[113] L. Curtin, A. Hawkins-Daarud, A.B. Porter, K.G. van der Zee, M.R. Owen, K.R. Swanson, A mechanistic investigation into ischemia-driven distal recurrence of glioblastoma, Bull. Math. Biol. 82 (11) (2020) 143, http://dx.doi.org/10.1007/s11538-020-00814-y.

[114] S. Tripathi, T. Vivas-Buitrago, R.A. Domingo, et al., IDH-wild-type glioblastoma cell density and infiltration distribution influence on supramarginal resection and its impact on overall survival: a mathematical model, J. Neurosurg. 136 (6) (2021) 1567–1575, http://dx.doi.org/10.3171/2021.6.JNS21925.

[115] B. Ocaña-Tienda, J. Pérez-Beteta, J.D. Villanueva-García, et al., A comprehensive dataset of annotated brain metastasis MR images with clinical and radiomic data, Sci. Data 10 (1) (2023) 208, http://dx.doi.org/10.1038/s41597-023-02123-0.

[116] A.W. Moawad, A. Janas, U. Baid, et al., The brain tumor segmentation (BraTS-METS) challenge 2023: Brain metastasis segmentation on pre-treatment MRI, 2023, Preprint: ArXiv; arXiv:2306.00838v1.

[117] D. Ramakrishnan, L. Jekel, S. Chadha, et al., A large open access dataset of brain metastasis 3D segmentations with clinical and imaging feature information, 2023, Preprint: ArXiv; arXiv:2309.05053.